

Partial Observability during DRL for Robot Control*

Lingheng Meng¹, Rob Gorbet² and Dana Kulić³

Abstract—Deep Reinforcement Learning (DRL) has made tremendous advances in both simulated and real-world robot control tasks in recent years. Nevertheless, applying DRL to novel robot control tasks is still challenging, especially when researchers have to design the action and observation space and the reward function. In this paper, we investigate partial observability as a potential failure source of applying DRL to robot control tasks, which can occur when researchers are not confident whether the observation space fully represents the underlying state. We compare the performance of three common DRL algorithms, TD3, SAC and PPO under various partial observability conditions. We find that TD3 and SAC become easily stuck in local optima and underperform PPO. We propose multi-step versions of the vanilla TD3 and SAC to improve robustness to partial observability based on one-step bootstrapping.

I. INTRODUCTION

Deep Reinforcement Learning (DRL) has been applied to both discrete and continuous control tasks, such as game playing [1], [2], [3], simulated robots [4], [5], and real world robots [6], [7], [8]. Although there have been tremendous advances in DRL, there are many challenges in applying DRL to real world robots [9], [10]. In this paper, we focus on partial observability of the observation space, which changes a given task from a Markov Decision Process (MDP) to a Partially Observable MDP (POMDP).

Many popular DRL algorithms are formulated for MDP problems. However, POMDP is common in novel and complex control tasks [11], [12], [13] due to lack of knowledge of the structure of the dynamics, sensor limitations, missing data, etc. In addition, most literature assumes that the key components of an environment, namely the action and observation space and the reward function, are given, which may not necessarily be true for complex systems. For DRL algorithms developed for handling POMDPs [14], [15], [16], [17], [18], researchers usually assume the tasks on hand are POMDPs, rather than first determining if the given tasks are POMDPs or MDPs. In real applications, these assumptions may not be satisfied. Therefore, researchers may encounter unexpected results that are different from those usually reported in literature with these assumptions.

*This work is supported by a SSHRC Partnership Grant in collaboration with Philip Beesley Studio, Inc.

¹Lingheng Meng is with Department of Electrical and Computer Engineering, University of Waterloo, 200 University Avenue West, Waterloo, ON, Canada lingheng.meng@uwaterloo.ca

²Rob Gorbet is with Departments of Knowledge Integration and Electrical and Computer Engineering, University of Waterloo, 200 University Avenue West, Waterloo, ON, Canada rob.gorbet@uwaterloo.ca

³Dana Kulić is with the Faculty of Engineering, Monash University, 14 Alliance Lane, Melbourne, Victoria, Australia dana.kulic@monash.edu

Moreover, researchers tend to present successes in applying DRL to robot control, but hide the failure stories behind these successes, the reason of these failures and how they detect them, which can be useful to make DRL approaches more useable in robotics.

This paper aims to fill the gap between directly assuming a novel system to be controlled is a MDP or POMDP. Particularly, we first introduce an exemplar robot control problem caused by partial observability on a novel complex system, then discuss the potential effect of multi-step bootstrapping on passing temporal information. After that, we propose two hypotheses and the corresponding algorithms to verify these hypotheses. In the experiments, we reproduce the counter-intuitive results observed from the complex system on classic control tasks to confirm that the problem is caused by partial observability. In addition, the results to verify our hypotheses are presented. Then, we discuss the limitations of this work.

II. RELATED WORKS

Multi-step methods have been investigated in the literature for improving reward signal propagation [19], [3], [20], [21] and alleviating the over-estimation problem [22]. However, as far as we know, there is no work connecting multi-step methods to their potential effect on passing temporal information when solving POMDP. In this work, we empirically show that multi-step bootstrapping helps TD3 and SAC to perform better on POMDPs.

POMDPs have been investigated within both model-free [14], [15], [18] and model-based [17], [23] DRL, where the tasks are known POMDPs. In this work, we do not focus on proposing new algorithms for solving POMDPs, but empirically show that when unsuccessfully applying DRLs to a complex control task the source of the failure may be related to partial observability, which is applicable to applications where researchers are not confident whether the given task is MDP or POMDP.

[24] studies the environment design, including the state representations, initial state distributions, reward structure, control frequency, episode termination procedures, curriculum usage, the action space, and the torque limits, that matter when applying DRL. They empirically show these design choices can affect the final performance significantly. In addition, [25] focuses on investigating the challenges of training real robots with DRL rather than simulated ones. [26] studies the factors that matter in learning from offline human demonstrations, where the observation space design is highlighted as one of the prominent aspects. These works aim to comprehensively cover broader topics in applying DRL, but in this work we mainly focus on the partial observability

problem during DRL for robot control. Moreover, we try to reproduce the problem encountered when applying DRL to novel robot on classic tasks that are accessible to everyone, as we understand many domain robots are not available to researchers who want to reproduce the experiment represented in many works.

III. BACKGROUND

Markov Decision Process (MDP): is a sequential decision process defined as a 4-tuple S, A, P, R , where S is the state space, A is the action space, $P(s'|s, a) = p(s_{t+1} = s' | s_t = s, a_t = a)$ is the transition probability that action a in state s at time t will lead to a new state s' at time $t + 1$, and $R(s, a, s') \in \mathbb{R}$ provides the immediate reward r indicating how good taking action a is in state s after transitioning to a new state s' . In MDP, it is assumed that the state transitions defined in P satisfy the Markov property, i.e. the next state s' only depends on the current state s and the action a . Normally, the state s is not accessible to an agent, but its representation o is given. When the observation o fully captures the current state s , we call this fully observable MDP. However, when the observation o cannot fully represent the current state s , we call the decision process Partially Observable Markov Decision Process (POMDP). For some cases, using a history of past observations and/or actions and/or rewards up to time t as a new observation can reduce a POMDP to MDP. For example, for tasks where the velocity is the key to solve a problem, using a history of past position of a robot as the observation can make the POMDP, where only position is included in its observation, a MDP. For these cases, history aids with dealing with partial observability.

Reinforcement Learning (RL): [27] studies how to solve MDPs or POMDPs, without requiring the transition dynamics P to be known. Specifically, an agent observes o_t at time t , then decides to take action a_t according to its current policy $a_t \sim \pi(a_t | o_t)$. Once the action a_t is taken, the agent observes a new observation o_{t+1} and receives a reward signal r_t from the environment. By continuously interacting with the environment, the agent learns an optimal policy π^* to maximize the expectation of the discount return $\mathbb{E}_{\pi^*, o_0 \sim \rho_0} [\sum_{t=0}^T \gamma^t r_t | o_0]$ starting from initial observation $o_0 \sim \rho_0$, where the discount factor γ is used to balance the short-term vs. long-term return.

There are three functions are commonly used in RL algorithms. A state-value function $V^\pi(s)$ of a state s under a policy π is the expected return when starting in s and following π thereafter, which can be formally defined by $V^\pi(s) = \mathbb{E}_\pi [\sum_{i=0}^{T-t} \gamma^i r_{t+i} | s_t = s]$. An action-value function $Q(s, a)$ of taking action a in state s and following π afterwards can be defined as $Q^\pi(s, a) = \mathbb{E}_\pi [\sum_{i=0}^{T-t} \gamma^i r_{t+i} | s_t = s, a_t = a]$. The advantage $A^\pi(s, a)$ of taking action a in state s is defined as $Q^\pi(s, a) - V^\pi(s)$ when following a policy π . For these functions, if the state s is not directly observable, its representation o will be used. To simplify the notation, for the rest of this paper, we will use o to represent s .

A. Deep Reinforcement Learning

Deep Reinforcement Learning (DRL) employs Deep Neural Networks to represent these value functions and/or policy. In this paper, we will use three of the most popular DRL algorithms which will be briefly introduced in the following.

Both *Soft Actor-Critic (SAC)* [28] and *Twin Delayed Deep Deterministic Policy Gradient (TD3)* [29] are off-policy actor-critic DRL and they both employ two neural networks to approximate two versions of the state-action value function (named *critics*) $Q_{i=1,2}$ parameterized by $\theta_{i=1,2}$. Learning two versions of the critic is used to address the function approximation error by taking the minimum over the bootstrapped Q-values in the next observation o_{t+1} . Different from TD3, SAC gives a bonus reward to an agent at each time step, proportional to the entropy of the policy at that timestep. In addition, TD3 learns a deterministic policy μ parameterized by ϕ , whereas SAC learns a stochastic policy π_ψ parameterized by ψ . Given a mini-batch of experiences (o_t, a_t, r_t, o_{t+1}) uniformly sampled from the replay buffer D , the target bootstrapped Q-value $\hat{Q}(o_t, a_t)$ of taking action a_t in observation o_t can be defined with the target networks as follows:

$$\hat{Q}(o_t, a_t) = r_t + \gamma \left[\min_{i=1,2} Q_{\theta_i^-}(o_{t+1}, a^-) + \alpha H(\pi(\cdot | s_{t+1})) \right] \quad (1)$$

where the target Q-value functions are parameterized by θ_i^- , $a^- = \mu_{\phi^-}(o_{t+1})$ for TD3 with target policy μ_{ϕ^-} and $a^- \sim \pi_{\psi^-}(a | o_{t+1})$ for SAC with target policy π_{ψ^-} , and $\alpha \geq 0$ balances the maximization of the accumulated reward and entropy. For TD3 $\alpha = 0$. Then, Q_i can be optimized by minimizing the expected difference between the prediction and the bootstrapped value with respect to parameters θ_i , following $\min_{\theta_i} \mathbb{E}_{(o_t, a_t, r_t, o_{t+1}) \sim D} [Q_{\theta_i}(o_t, a_t) - \hat{Q}(o_t, a_t)]^2$. For TD3, the policy is optimized by maximizing the expected Q-value over the mini-batch of o_t with respect to the policy parameter ϕ , following $\max_{\phi} \mathbb{E}_{o_t \sim D} Q_{\theta_1}(o_t, \mu_{\phi}(o_t))$, and for SAC the policy is updated to maximize the expected Q-value on o_t, a where a is sampled from policy $\pi_{\psi}(\cdot | o_t)$ and the expected entropy of π in observation o_t as $\max_{\psi} \mathbb{E}_{o_t \sim D} [\min_{i=1,2} Q_{\theta_i}(o_t, a) |_{a \sim \pi_{\psi}(a | o_t)} + \alpha H(\pi_{\psi}(\cdot, o_t))]$.

Proximal Policy Optimization (PPO) [30] optimizes a policy by taking the biggest possible improvement step using the data collected by the current policy, but at the same time limiting the step size to avoid performance collapse. A common way to achieve this is to attenuate policy adaptation. Formally, for a set of observation and action pairs (o_t, a_t) collected from the environment based on the current policy π_{ϕ_k} , the new policy π_{ϕ} is obtained by maximizing the expectation over the loss function $L(o_t, a_t, \phi_k, \phi)$ with respect to the policy parameter ϕ as $\max_{\phi} \mathbb{E}_{(o_t, a_t) \sim \pi_{\phi_k}} L(o_t, a_t, \phi_k, \phi)$. The loss function L is defined as $L(o_t, a_t, \phi_k, \phi) = \min \left(\frac{\pi_{\phi}(a_t | o_t)}{\pi_{\phi_k}(a_t | o_t)} A^{\pi_{\phi_k}}(o_t, a_t), \text{clip} \left(\frac{\pi_{\phi}(a_t | o_t)}{\pi_{\phi_k}(a_t | o_t)}, 1 - \varepsilon, 1 + \varepsilon \right) A^{\pi_{\phi_k}}(o_t, a_t) \right)$, where ε is a small hyperparameter that roughly says how far away the new policy is allowed to go from the current one, and $A^{\pi_{\phi_k}}(o_t, a_t)$ is the advantage value. A common

way to estimate the advantage is called generalized advantage estimator GAE(λ) [31], based on the λ -return and the estimated state-value $V(o_t)$ in observation o_t as $A^{\gamma\phi_k}(o_t, a_t) = R_t(\lambda) - V_v(o_t)$. The $R_t(\lambda)$ is defined by

$$R_t(\lambda) = (1 - \lambda) \sum_{n=1}^{T-t-1} \lambda^{n-1} R_t^{(n)} + \lambda^{T-t-1} R_t^{(T-t)} \quad (2)$$

where $\lambda \in [0, 1]$ balances the weights of different multi-step returns and the summation of the coefficients satisfies $1 = (1 - \lambda) \sum_{n=1}^{T-t-1} \lambda^{n-1} + \lambda^{T-t-1}$. Particularly, $R_t^{(n)}$ is defined as $R_t^{(n)} = \sum_{i=t}^{t+n-1} \gamma^{i-t} r_i + \gamma^n V_v(o_{t+n})$ that is bootstrapped by state-value $V_v(o_{t+n})$ in observation o_{t+n} . The state-value function V_v is optimized to minimize the mean-square-error between the predicted state value $V_v(o_t)$ and the Monte-Carlo return $R_t = \sum_{i=t}^T \gamma^{i-t} r_i$ based on the experiences collected by the current policy, as $\min_v \mathbb{E}_{o_t} [V_v(o_t) - R_t]^2$.

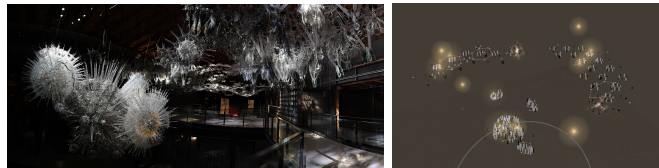
Multi-step Methods (also called n -step methods) [27] refer to RL algorithms utilizing multi-step bootstrapping. Formally, for a multi-step bootstrapping where n is the step size after which bootstrapped value will be used, the n -step bootstrapping of observation and action pair (o_t, a_t) can be defined as $Q^{(n)}(o_t, a_t) = \sum_{i=t}^{t+n-1} \gamma^{i-t} r_i + \gamma^n Q(o_{t+n}, a)$ where $a \sim \pi(a|o_{t+n})$. Note that when $n = 1$, it reduces to 1-step bootstrapping, which is commonly used in Temporal Deference (TD) based RL.

IV. EXEMPLAR ROBOT CONTROL PROBLEM

In this section, we will provide a motivating example highlighting the challenge of applying DRL to complex robotic control tasks. The Living Architecture System (LAS) [32], [33], an architectural-scale interactive system with hundreds of actuators such as lights, shaped memory alloys, DC motors and speakers, etc., and sensors such as infrared sensors and microphones, etc., is a robot system that is: (1) novel, i.e., not a commonly used as test-bed in DRL, requiring researchers to design the action/observation space and reward function; and (2) complex, i.e., the dynamics of the robot itself and its external environment is unknown. LAS is designed by a collection of architects, artists, psychologists, roboticists, computer scientists and engineers, aiming to engage occupants in a long-term interaction. A classic scenario in LAS is multiple visitors wandering around a LAS and trying to interact with it, where the long-term goal is to engage the visitors without boring them. Fig. 1 shows a LAS installation *Meander*¹, where Fig. 1a shows a photo of the physical installation and Fig. 1b shows the simulated *Meander* within LAS-Behavior-Engine, a simulator and a behavior controller. Within the LAS, there are over 500 actuators and about 50 sensors spread over the whole space of the installation. With such a large set of actuators and sensors and the complexity of human factors, it is extremely hard to handcraft engaging behavior by direct control of the actuators. Therefore, a middle layer is designed to add a set of dynamics to induce different

¹More images and demonstrative videos of *Meander* can be found in <https://youtu.be/SVTc7xOSBrq>.

activation intensities in the actuators either when observing changes in sensors or when in background behavior mode. The parameters involved in controlling the dynamics can be used by either human designers or learning agents to generate engaging behaviors in the LAS. In other words, the large raw action space is transferred by a complex dynamics into a simplified and easy-to-understand parameterized action space. For example, in Fig. 1b the excitors (yellow spheres) are randomly positioned and attracted to move to attractors (pink hexagons) and activate actuators they pass by as they do so, which are controlled by parameters such as the size, the speed and the maximum number of excitors, etc.



(a) Physical LAS (b) Simulated LAS

Fig. 1: LAS installation *Meander*, where (a) is an image of the physical installation *Meander* (courtesy of Philip Beesley Studio Inc.), and (b) shows the simulated LAS.

To apply DRL to LAS, researchers need to design the key RL components, namely the observation and action space and the reward function. However, the design of these components is not trivial. In a first attempt to learn an effective control policy, we designed the three components of LAS as: **Observation space**: the status of actuators and sensory readings in $[0, 1]$ within a time window. Specifically, for a 1 second time window and 1Hz data reading, the observation space has 724 dimensions, composed of 124 dimensions of sensory readings and 600 dimensions of actuator status; **Action space**: the 9 dimensional parameterized action space in $[-1, 1]$ where each dimension corresponds to one parameter involved in the excitor dynamics and applies to all excitors within the system; and **Reward function**: the average over the actuator intensities included in the observation space, which means the reward function encourages actions that maximally activate the actuators.

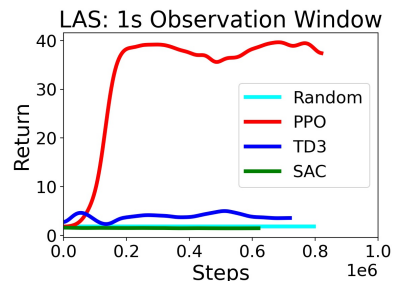


Fig. 2: Unexpected Results on LAS, where PPO is better than TD3 and SAC.

Three state-of-the-art DRL algorithms, i.e. TD3, SAC, and PPO, introduced in Section III were tested on the environment. Fig. 2 shows the learning curves of these

algorithms on LAS with the observation, action and reward formulated as described above. Surprisingly, TD3 and SAC perform much worse than PPO, where TD3 is slightly better than random and SAC is about the same as random, contrary to reports that the performance of both TD3 and SAC are much better than PPO on tasks provided in OpenAI Gym [29], [28].

After some investigation, we found that the problem shown in Fig. 2 is caused by the the partial observability of the observation space². Temporal information is unavailable through the 1s observation window, but somehow PPO seems to be able to incorporate some temporal information while TD3 and SAC fail. To be more concrete, when the observation window is 1s, there is no any information about the change rate of the actuator status and the sensory reading, which may be important to the problem solving. For example, knowing the increase or decrease of the activation intensity of an acutar caused by an action is beneficial to learn a policy that encourages active behavior. However, intuitively, TD3, SAC and PPO are all general DRL alirhtms without special consideration for handling POMDP. To interpret these results we identify variations on benchmark OpenAI gym tasks that replicate the algorithms’ performance.

V. THE POTENTIAL EFFECT OF MULTI-STEP BOOTSTRAPPING ON PASSING TEMPORAL INFORMATION

To understand why PPO is better than TD3 and SAC in terms of handling POMDP, we revisit their policy and value function optimization introduced in Section III. One prominent difference among them is that PPO uses multi-step bootstrapping with $n > 1$ while TD3 and SAC use 1-step bootstrapping. Specifically, PPO uses λ -return defined in Eq. 2, which is a weighed average of n -step returns where $n \in [1, T - t - 1]$, to calculate the advantage $A^{\pi_{\phi_k}}(o_t, a_t)$ of taking action a_t in observation o_t . However, TD3 and SAC only use 1-step bootstrapping to calculate their target Q-value as defined in Eq. 1.

The reward signal $r = R(o, a, o')$ can be seen as a one-dimensional state-transition abstraction of (o, a, o') . If the reward signal is dense, it is possible that each underlying state can be uniquely represented by a reward signal. Then, for the case where $R(o, a_1, o'_1) < R(o, a_2, o'_2)$, a_1 can be thought to encode less information than a_2 . Therefore, the goal of an agent can be interpreted to maximize accumulated information encoding. With n -step bootstrapping where $n > 1$, n consecutive state-transition abstractions are combined through weighted summation. By combining consecutive state-transition abstractions, some temporal information is also incorporated. One may argue that even for $n = 1$ it is also possible to incorporate temporal information that exists in the value function. However, the value function is approximate, which is not as effective as that calculated directly from the

²Along with environment related hyper-parameters such as observation and action space and reward function design, without thorough RL algorithm related hyper-parameter search, we did try to reduce the depth of the neural networks employed in TD3 and SAC, but did not find an obvious difference in the performance.

n consecutive state-transition abstractions. Once the n -step bootstrapping has incorporated temporal information, it will be passed to the value function. When the policy is optimized based the value function, it will be further passed to the policy as well.

VI. HYPOTHESES VERIFICATION

Based on the aforementioned unexpected results and the analysis, we make two hypotheses:

Hypothesis 1: If partial observability caused the unexpected results in Section IV, then similar results should be reproducible on MDP vs. POMDP versions of benchmark tasks.

Hypothesis 2: The λ -return (Eq. 2) based on n -step bootstrapping employed in PPO leads to robustness to POMDP, therefore (1) n -step version of TD3 and SAC with $n > 1$ should also improve robustness to POMDP compared to their vanilla versions, and (2) replacing λ -return with 1-step bootstrapping should cause PPO’s performance to decrease when moving from MDP to POMDP.

To empirically verify the hypotheses, we propose Multi-step TD3 (MTD3) and Multi-step SAC (MSAC). Firstly, instead of sampling a mini-batch $\left\{ (o_t, a_t, r_t, o_{t+1})^{(k)} \right\}_{k=1}^K$ of K 1-step experiences, we sample a mini-batch $\left\{ (o_t, a_t, r_t, o_{t+1}, \dots, o_{t+n-1}, a_{t+n-1}, r_{t+n-1}, o_{t+n})^{(k)} \right\}_{k=1}^K$ of K n -step experiences. Then, we replace the target Q-value calculation defined in Eq. 1 with the n -step bootstrapping defined as $\hat{Q}^{(n)}(o_t, a_t) = \sum_{i=t}^{t+n-1} \gamma^{i-t} r_i + \gamma^n \left[\min_{i=1,2} Q_{\theta_i^-}(o_{t+n}, a) + \alpha H(\pi(\cdot | o_{t+n})) \right]$, where $a = \mu_{\phi^-}(o_{t+n})$ and $a \sim \pi_{\psi^-}(a | o_{t+n})$ for MTD3 and MSAC, respectively, $\alpha = 0$ for MTD3, and the policy update is the same as that for TD3 and SAC.

VII. EXPERIMENTS

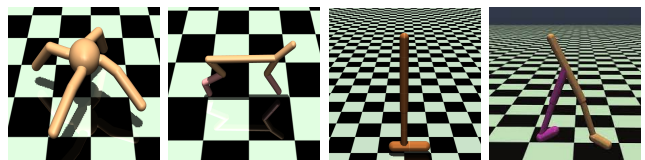


Fig. 3: Classic Tasks.

TABLE I: MDP- and POMDP-version of Classic Tasks

Name	Description	Hyper-parameter
MDP	Original task	–
POMDP-RV	Remove all velocity-related entries in the observation space.	–
POMDP-FLK	Reset the whole observation to 0 with probability p_{flk} .	$p_{flk} = 0.2$
POMDP-RN	Add random noise $\varepsilon \sim \mathbb{N}(0, \sigma_m)$ to each entry of the observation.	$\sigma_m = 0.1$
POMDP-RSM	Reset an entry of the observation to 0 with probability p_{rsm} .	$p_{rsm} = 0.1$

TABLE II: The Maximum of Average Return over 5 evaluation episodes within 2 million steps based on 3 different random seeds. To ease the comparison, if TD3 or SAC perform worse than PPO, they will be gray-colored. If MTD3(5) or MSAC(5) outperforms corresponding TD3 or SAC, they will be red-colored. The maximum value of all evaluated algorithms for each task is bolded.

Task		Algorithms					
Name	Version	PPO	TD3	SAC	MTD3(5)	MSAC(5)	LSTM-TD3(5)
Ant	MDP	1315.61	5976.49	6106.42	4174.73	5474.10	4745.36
	POMDP-FLK	1087.93	1339.88	972.37	2154.18	4205.45	3420.69
	POMDP-RN	587.87	1684.48	1431.37	1315.31	3185.56	1130.96
	POMDP-RSM	836.34	1737.50	931.68	2819.81	4204.35	1459.67
	POMDP-RV	3412.95	1870.12	1102.99	3123.41	4160.47	1958.36
HalfCheetah	MDP	3770.88	11345.21	11887.53	7001.51	8694.46	10086.52
	POMDP-FLK	2183.27	1377.18	248.49	1289.14	4803.40	1678.92
	POMDP-RN	3975.56	5306.12	4651.56	5503.61	5865.68	4395.61
	POMDP-RSM	3338.03	1395.06	123.70	3314.96	5847.08	1467.68
	POMDP-RV	4120.39	2937.80	498.51	3955.83	4017.05	4406.33
Hopper	MDP	3604.01	3823.88	3993.51	3700.19	4065.26	3677.02
	POMDP-FLK	2657.15	1043.63	1047.01	1219.17	1048.73	3587.02
	POMDP-RN	3469.32	2125.03	1026.52	3022.95	3318.88	3426.28
	POMDP-RSM	3107.39	2506.26	1003.19	3187.08	3184.48	1169.30
	POMDP-RV	2613.43	1023.38	1119.84	1000.27	1144.11	592.39
Walker2d	MDP	4230.38	5762.66	6097.24	7181.57	5615.33	5189.87
	POMDP-FLK	2723.41	999.17	1003.27	1243.08	1412.80	4219.05
	POMDP-RN	4160.27	1220.65	1060.09	3959.90	3977.56	4191.02
	POMDP-RSM	3295.34	2178.42	2009.92	4197.03	4778.27	4083.16
	POMDP-RV	3531.14	1443.01	2199.88	2670.89	3397.12	4356.57

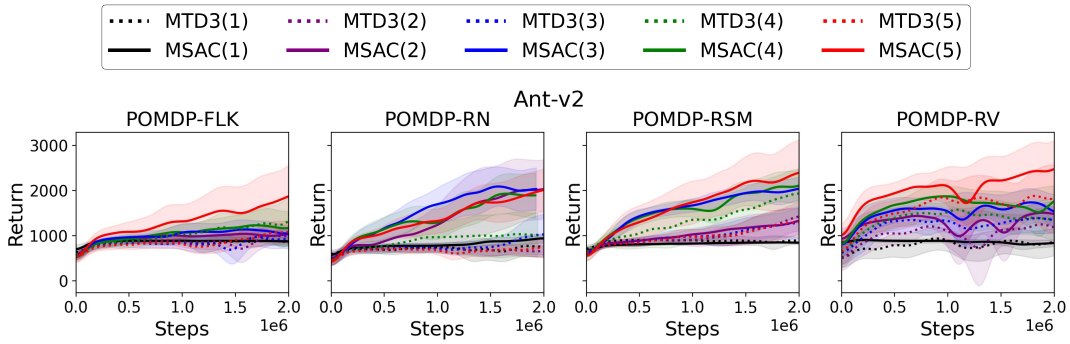


Fig. 4: Effect of Multi-step Size on The Performance of MTD3 and MSAC, where the average learning curves correspond to MTD3(n) and MSAC(n) with different multi-step sizes n and the shaded area shows half of standard deviation of the average accumulated return over 3 random seeds.

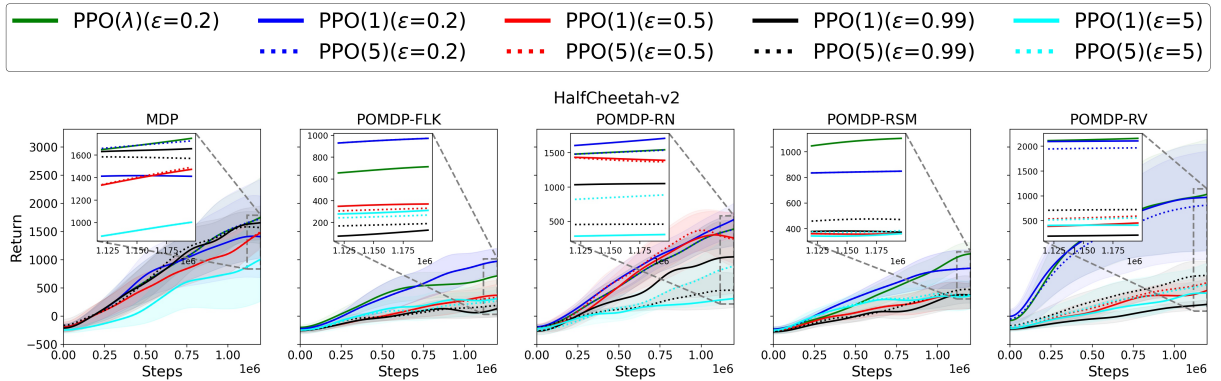


Fig. 5: Effect of Multi-step Size on The Performance of PPO, where the average learning curves correspond to PPO(λ) with λ -return and PPO(n) with simple n -step bootstrapping and the shaded area shows half of standard deviation of the average accumulated return over 3 random seeds. The ϵ indicates how far away the new policy is allowed to go from the current one.

Fig. 3 shows the classic MuJoCo tasks (Ant-v2, HalfCheetah-v2, Hopper-v2, Walker2d-v2) from OpenAI Gym that we will use to reproduce the aforementioned results on LAS, and Table I shows their POMDP-versions proposed in [18]. Note that the POMDP-version tasks only transform the observation space of the original task, but leave the reward signal unchanged, which means the reward signal is still based on the original observations. This enables fair comparison among the performances of an agent on MDP and POMDP. The neural network structures and hyper-parameters of PPO, TD3, SAC, MTD3(n), MSAC(n) are the same as the implementation in OpenAI Spinning Up (<https://spinningup.openai.com>), and the source code of this paper can be found in https://github.com/LinghengMeng/m_rl_pomdp. The n in the bracket indicates the step size in multi-step bootstrapping. LSTM-TD3(l) [18] is also compared to see how the MTD3(n) and MSAC(n) perform compared to an algorithm specifically designed for dealing with POMDP, where l indicates the memory length. The results shown in this section are based on three random seeds. For better visualization, learning curves are smoothed by 1-D Gaussian filter with $\sigma = 20$.

A. Experiment Results on Classic Tasks

Table II shows the maximum of average return of PPO, TD3, SAC, MTD3(5), MSAC(5) and LSTM-TD3(5) calculated over 5 episodes. Firstly, to verify **Hypothesis 1** and comparing PPO, TD3 and SAC, we found that: (1) TD3 and SAC significantly outperform PPO on all MDP tasks; (2) TD3 and SAC are much worse than PPO on most POMDP tasks. In addition, (3) TD3 and SAC experience dramatic drops in performance when moving from MDP to POMDP, while PPO does not experience too much change in performance. These observations match perfectly the unexpected results described in Section IV, indicating that the problem comes from the partial observability.

When we compare TD3 and SAC to their multi-step versions MTD3(5) and MSAC(5) on POMDPs in Table II, it can be seen that MTD3(5) and MSAC(5) outperform their vanilla versions on most POMDPs (highlighted in red in Table II), which verifies **Hypothesis 2 (1)**. Even though MTD3(5) and MSAC(5) show performance increase compared to TD3 and SAC and comparable or better performance than PPO on POMDPs, LSTM-TD3(5) exhibits dramatically better performance on some tasks, e.g. POMDP-FLK of Walker2d-v2 and Hopper-v2. This indicates that for some cases directly learning a good representation of the underlying state from a short experience trajectory is more effective than relying on multi-step bootstrapping to pass some temporal information. Fig. 4 shows the average learning curves of MTD3(n) and MSAC(n) with different multi-step sizes $n = \{1, 2, 3, 4, 5\}$, when $n = 1$ they reduce to TD3 and SAC. It can be seen from Fig. 4 that simply increasing n by a few steps makes their performance dramatically better than $n = 1$ with a little extra computation cost. For the n we tested, $n = 5$ shows the best performance on most tasks.

Fig. 5 compares PPO(λ) with λ -return and PPO(n) with simple n -step bootstrapping. From this figure, we observe that when λ -return is replaced with 1-step bootstrapping, the performance of PPO does not change much, which rejects **Hypothesis 2 (2)**. Compared to the return estimation, when the clip ratio ϵ is increased, PPO’s performance experiences a significant decrease. In summary, the results shown in this section support **Hypothesis 1**, but for **Hypothesis 2** only the first part is supported by the results.

VIII. LIMITATIONS

We empirically demonstrated that multi-step bootstrapping has a role to play in solving POMDP by employing classic tasks from OpenAI Gym with some modification on the observation space to create POMDPs. Because the observation space of these classic tasks is very small compared to real world applications, we are not confident if the finding in this paper generalizes well to other applications. Even though we explained why multi-step bootstrapping can pass temporal information by interpreting the reward signal as a one-dimensional state-transition abstraction, a stronger and clearer justification of why multi-step bootstrapping helps with handling temporal information is important to understand the underlying mechanism, especially given that **Hypothesis 2** is only partially supported by the results, which will be left to the future study.

IX. CONCLUSION AND FUTURE WORKS

In this paper, we first highlight the counter-intuitive observation found when applying DRLs to a novel complex robot, that PPO outperforms TD3 and SAC. We hypothesize that this degradation in performance is caused by partial observability. Then, we provide a potential explanation about why the multi-step bootstrapping employed in PPO makes it more robust to partial observability compared TD3 and SAC, which only rely on 1-step bootstrapping. Based on that, we proposed MTD3 and MSAC to verify our hypotheses on MDP- and POMDP-version of classic tasks. The same counter-intuitive observation can be reproduced on the POMDP-versions of the classic tasks, which confirms the problem is caused by partial observability. The results of MTD3 and MSAC with multi-step size $n = 5$ show that simply increasing the step size from $n = 1$ to $n = 5$ can significantly increase the performance of vanilla TD3 and SAC on POMDPs.

A deeper understanding about why n -step bootstrapping can make TD3 and SAC better on POMDP is an interesting direction for the future. Besides, it is also worth to investigate if LSTM-TD3 and MTD3 can be combined to allow TD3 to solve POMDP better by learning temporal information both from the past experiences and from the future rewards.

ACKNOWLEDGMENT

This research was enabled in part by support provided by Compute Canada (www.computecanada.ca). Lingheng would like to thank Matt Gorbet and Michael Lancaster for their help with the setup of the LAS simulator.

REFERENCES

- [1] V. Mnih, K. Kavukcuoglu, D. Silver, A. Graves, I. Antonoglou, D. Wierstra, and M. Riedmiller, "Playing atari with deep reinforcement learning," *arXiv preprint arXiv:1312.5602*, 2013.
- [2] V. Mnih, K. Kavukcuoglu, D. Silver, A. A. Rusu, J. Veness, M. G. Bellemare, A. Graves, M. Riedmiller, A. K. Fidjeland, G. Ostrovski, et al., "Human-level control through deep reinforcement learning," *nature*, vol. 518, no. 7540, pp. 529–533, 2015.
- [3] V. Mnih, A. P. Badia, M. Mirza, A. Graves, T. Lillicrap, T. Harley, D. Silver, and K. Kavukcuoglu, "Asynchronous methods for deep reinforcement learning," in *International conference on machine learning*. PMLR, 2016, pp. 1928–1937.
- [4] T. P. Lillicrap, J. J. Hunt, A. Pritzel, N. Heess, T. Erez, Y. Tassa, D. Silver, and D. Wierstra, "Continuous control with deep reinforcement learning," *arXiv preprint arXiv:1509.02971*, 2015.
- [5] Y. Duan, X. Chen, R. Houthoofd, J. Schulman, and P. Abbeel, "Benchmarking deep reinforcement learning for continuous control," in *International conference on machine learning*. PMLR, 2016, pp. 1329–1338.
- [6] L. Tai, G. Paolo, and M. Liu, "Virtual-to-real deep reinforcement learning: Continuous control of mobile robots for mapless navigation," in *2017 IEEE/RSJ International Conference on Intelligent Robots and Systems (IROS)*. IEEE, 2017, pp. 31–36.
- [7] A. R. Mahmood, D. Korenkevych, G. Vasan, W. Ma, and J. Bergstra, "Benchmarking reinforcement learning algorithms on real-world robots," in *Conference on robot learning*. PMLR, 2018, pp. 561–591.
- [8] S. Satheeshbabu, N. K. Uppalapati, T. Fu, and G. Krishnan, "Continuous control of a soft continuum arm using deep reinforcement learning," in *2020 3rd IEEE International Conference on Soft Robotics (RoboSoft)*. IEEE, 2020, pp. 497–503.
- [9] P. Henderson, R. Islam, P. Bachman, J. Pineau, D. Precup, and D. Meger, "Deep reinforcement learning that matters," in *Proceedings of the AAAI conference on artificial intelligence*, vol. 32, no. 1, 2018.
- [10] G. Dulac-Arnold, N. Levine, D. J. Mankowitz, J. Li, C. Paduraru, S. Gowal, and T. Hester, "Challenges of real-world reinforcement learning: definitions, benchmarks and analysis," *Machine Learning*, vol. 110, no. 9, pp. 2419–2468, 2021.
- [11] A. R. Cassandra, "A survey of pomdp applications," in *Working notes of AAAI 1998 fall symposium on planning with partially observable Markov decision processes*, vol. 1724, 1998.
- [12] A. Foka and P. Trahanias, "Real-time hierarchical pomdps for autonomous robot navigation," *Robotics and Autonomous Systems*, vol. 55, no. 7, pp. 561–571, 2007.
- [13] S. C. Ong, S. W. Png, D. Hsu, and W. S. Lee, "Pomdps for robotic tasks with mixed observability," in *Robotics: Science and systems*, vol. 5, 2009, p. 4.
- [14] M. Hausknecht and P. Stone, "Deep recurrent q-learning for partially observable mdps," in *2015 aaai fall symposium series*, 2015.
- [15] G. Lample and D. S. Chaplot, "Playing fps games with deep reinforcement learning," in *Thirty-First AAAI Conference on Artificial Intelligence*, 2017.
- [16] P. Zhu, X. Li, P. Poupart, and G. Miao, "On improving deep reinforcement learning for pomdps," *arXiv preprint arXiv:1704.07978*, 2017.
- [17] M. Igl, L. Zintgraf, T. A. Le, F. Wood, and S. Whiteson, "Deep variational reinforcement learning for pomdps," in *International Conference on Machine Learning*. PMLR, 2018, pp. 2117–2126.
- [18] L. Meng, R. Gorbet, and D. Kulić, "Memory-based deep reinforcement learning for pomdps," in *2021 IEEE/RSJ International Conference on Intelligent Robots and Systems (IROS)*. IEEE, 2021, pp. 5619–5626.
- [19] H. van Seijen, "Effective multi-step temporal-difference learning for non-linear function approximation," *arXiv preprint arXiv:1608.05151*, 2016.
- [20] K. De Asis, J. Hernandez-Garcia, G. Holland, and R. Sutton, "Multi-step reinforcement learning: A unifying algorithm," in *Proceedings of the AAAI Conference on Artificial Intelligence*, vol. 32, no. 1, 2018.
- [21] M. Hessel, J. Modayil, H. Van Hasselt, T. Schaul, G. Ostrovski, W. Dabney, D. Horgan, B. Piot, M. Azar, and D. Silver, "Rainbow: Combining improvements in deep reinforcement learning," in *Thirty-second AAAI conference on artificial intelligence*, 2018.
- [22] L. Meng, R. Gorbet, and D. Kulić, "The effect of multi-step methods on overestimation in deep reinforcement learning," in *2020 25th International Conference on Pattern Recognition (ICPR)*. IEEE, 2021, pp. 347–353.
- [23] G. Singh, S. Peri, J. Kim, H. Kim, and S. Ahn, "Structured world belief for reinforcement learning in pomdp," in *International Conference on Machine Learning*. PMLR, 2021, pp. 9744–9755.
- [24] D. Reda, T. Tao, and M. van de Panne, "Learning to locomote: Understanding how environment design matters for deep reinforcement learning," in *Motion, Interaction and Games*, 2020, pp. 1–10.
- [25] J. Ibarz, J. Tan, C. Finn, M. Kalakrishnan, P. Pastor, and S. Levine, "How to train your robot with deep reinforcement learning: lessons we have learned," *The International Journal of Robotics Research*, vol. 40, no. 4-5, pp. 698–721, 2021.
- [26] A. Mandlekar, D. Xu, J. Wong, S. Nasiriany, C. Wang, R. Kulkarni, L. Fei-Fei, S. Savarese, Y. Zhu, and R. Martín-Martín, "What matters in learning from offline human demonstrations for robot manipulation," *arXiv preprint arXiv:2108.03298*, 2021.
- [27] R. S. Sutton and A. G. Barto, *Reinforcement learning: An introduction*. MIT press, 2018.
- [28] T. Haarnoja, A. Zhou, P. Abbeel, and S. Levine, "Soft actor-critic: Off-policy maximum entropy deep reinforcement learning with a stochastic actor," in *International conference on machine learning*. PMLR, 2018, pp. 1861–1870.
- [29] S. Fujimoto, H. Hoof, and D. Meger, "Addressing function approximation error in actor-critic methods," in *International conference on machine learning*. PMLR, 2018, pp. 1587–1596.
- [30] J. Schulman, F. Wolski, P. Dhariwal, A. Radford, and O. Klimov, "Proximal policy optimization algorithms," *arXiv preprint arXiv:1707.06347*, 2017.
- [31] J. Schulman, P. Moritz, S. Levine, M. Jordan, and P. Abbeel, "High-dimensional continuous control using generalized advantage estimation," *arXiv preprint arXiv:1506.02438*, 2015.
- [32] P. Beesley, *Near-living Architecture: Work in Progress from the Hylozoic Ground Collaboration, 2011-2013*. Riverside Architectural Press Toronto, Ontario, Canada, 2014.
- [33] L. Meng, D. Lin, A. Francey, R. Gorbet, P. Beesley, and D. Kulić, "Learning to engage with interactive systems: A field study on deep reinforcement learning in a public museum," *ACM Transactions on Human-Robot Interaction (THRI)*, vol. 10, no. 1, pp. 1–29, 2020.

Partial Observability during DRL for Robot Control: Supplementary Material*

Lingheng Meng¹, Rob Gorbet² and Dana Kulić³

Abstract—This manuscript is the supplementary material for the paper “Partial Observability during DRL for Robot Control” by Lingheng Meng, Rob Gorbet and Dana Kulić. It provides additional implementation details, and complementary results.

I. THE POTENTIAL EFFECT OF MULTI-STEP BOOTSTRAPPING ON PASSING TEMPORAL INFORMATION

Table I summarises the meaning of the key components of RL under the original and new interpretation of the reward function.

II. ALGORITHMS IMPLEMENTATION

The implementation of the algorithms is based on OpenAI Spinningup¹ and [1]. The code used for this work can be found in https://github.com/LinghengMeng/m_rl_pomdp. Table II details the hyperparameters used in this work, where – indicates the parameter does not apply to the corresponding algorithm. For the actor and critic neural network structure of LSTM-TD3, the first row corresponds to the structure of the memory component, the second row corresponds to the structure of the current feature extraction, and the third row corresponds to the structure of perception integration after combining the extracted memory and the extracted current feature.

III. EXPERIMENT RESULTS ON CLASSIC TASKS

Fig. 1 shows the learning curves of PPO, TD3, SAC, MTD(5), MSAC(5) and LSTM-TD3(5). Fig. 2 shows the learning curves of MTD3(n) and MSAC(n) with different $n = 1, 2, 3, 4, 5$. Fig. 3 shows the learning curves of PPO(λ) and PPO(n) with different $n = 1, 5$, where ϵ is the policy clip ratio.

REFERENCES

- [1] L. Meng, R. Gorbet, and D. Kulić, “Memory-based deep reinforcement learning for pomdps,” in *2021 IEEE/RSJ International Conference on Intelligent Robots and Systems (IROS)*. IEEE, 2021, pp. 5619–5626.
- [2] D. P. Kingma and J. Ba, “Adam: A method for stochastic optimization,” *arXiv preprint arXiv:1412.6980*, 2014.

*This work is supported by a SSHRC Partnership Grant in collaboration with Philip Beesley Studio, Inc.

¹Lingheng Meng is with Department of Electrical and Computer Engineering, University of Waterloo, 200 University Avenue West, Waterloo, ON, Canada lingheng.meng@uwaterloo.ca

²Rob Gorbet is with Departments of Knowledge Integration and Electrical and Computer Engineering, University of Waterloo, 200 University Avenue West, Waterloo, ON, Canada rob.gorbet@uwaterloo.ca

³Dana Kulić is with the Faculty of Engineering, Monash University, 14 Alliance Lane, Melbourne, Victoria, Australia dana.kulic@monash.edu

¹<https://spinningup.openai.com>

TABLE I: Interpretations of Reward Function

	Original Interpretation	New Interpretation
$R(o, a, o')$	the reward of taking action a in observation o which leading to a new observation o'	the 1 dimensional state-transition abstraction of taking action a in observation o leading to a new observation o' (a state-transition abstraction feature)
$Q^\pi(o, a)$	the expectation of the accumulated discounted reward when taking action a in observation o and following policy π thereafter	the expectation of the accumulated discounted state-transition abstraction when taking action a in observation o and following policy π thereafter
$V^\pi(o)$	the expectation of the accumulated discounted reward when in observation o and following policy π thereafter	the expectation of the accumulated discounted state-transition abstraction when in observation o and following policy π thereafter
$\pi(a o)$	policy π that is optimized to maximize the accumulated discounted reward	policy π that is optimized to maximize the accumulated discounted data representation

TABLE II: Hyperparameters for Algorithms

Hyperparameter	Algorithms					
	PPO	TD3	MTD3	SAC	MSAC	LSTM-TD3
discount factor: γ	0.99					
λ -return: λ	0.97	-				
clip ratio: ϵ	0.2	-				
batch size: N_{batch}	-	100				
replay buffer size: $ D $	4000	10^6				
random start step: N_{start_step}	-	10000				
update after N_{update_after}	-	1000				
target NN update rate τ	-	0.005				
optimizer	Adam [2]					
actor learning rate lr_{actor}	$3 * 10^{-4}$	10^{-3}				
critic learning rate lr_{critic}	10^{-3}	10^{-3}				
actor NN structure:	[256, 256]					$[128] + [128]$ [128] [128, 128]
critic NN structure:	[256, 256]					$[128] + [128]$ [128] [128, 128]
actor exploration noise σ_{act}	-	0.1		-	-	0.1
target actor noise σ_{targ_act}	-	0.2	0.2	-	-	0.2
target actor noise clip boundary c_{targ_act}	-	0.5	0.5	-	-	0.5
policy update delay	-	2	2	-	-	2
entropy regulation coefficient α	-	-	-	0.2	0.2	-
history length l	-	-	-	-	-	{0, 1, 3, 5}
bootstrapping step size n	-	-	{2, 3, 4, 5}	-	{2, 3, 4, 5}	-

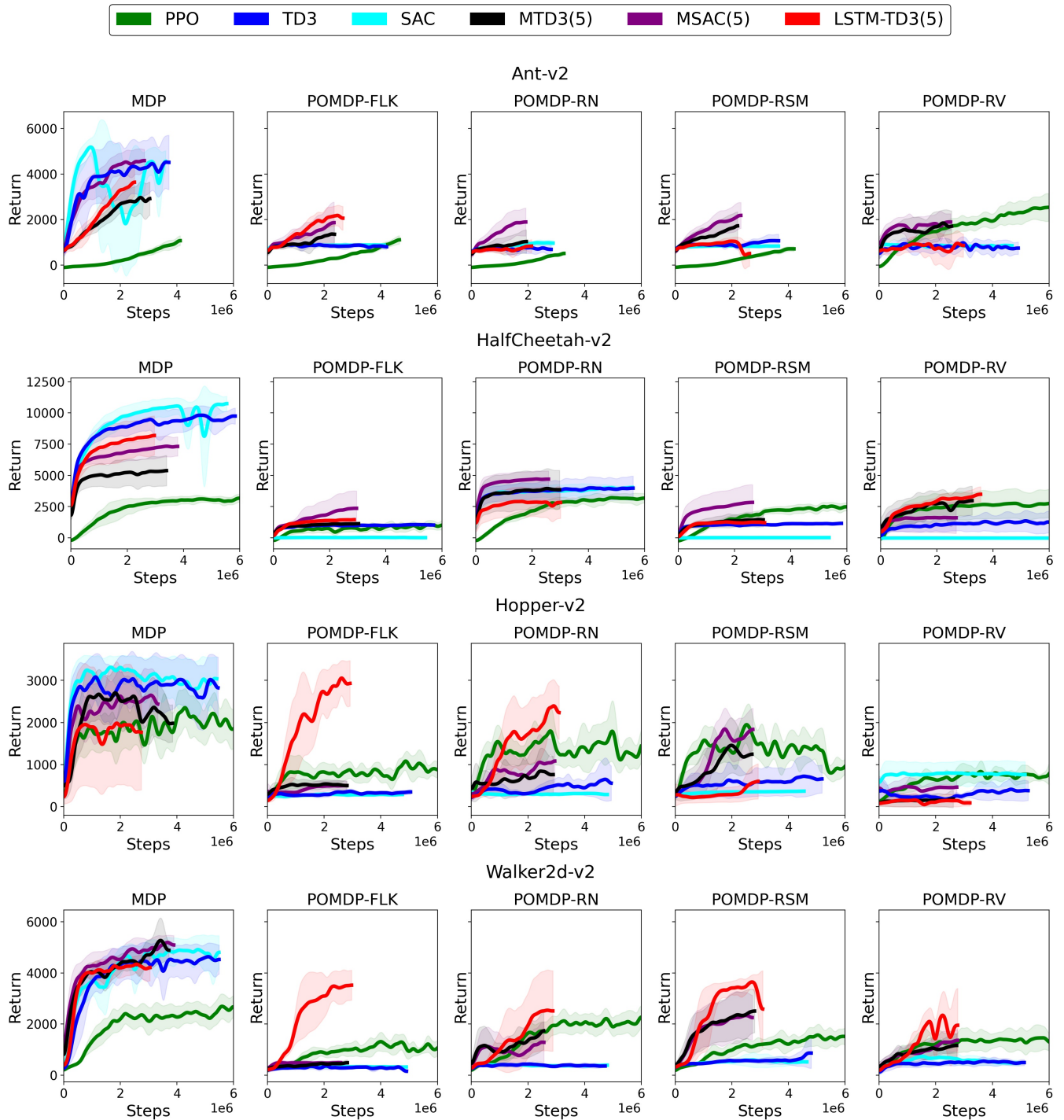


Fig. 1: Average Learning Curves on Classic Tasks, where the shaded area shows half of standard deviation of the average accumulated return over 3 random seeds. For better visualization, learning curves are smoothed by 1-D Gaussian filter with $\sigma = 20$.

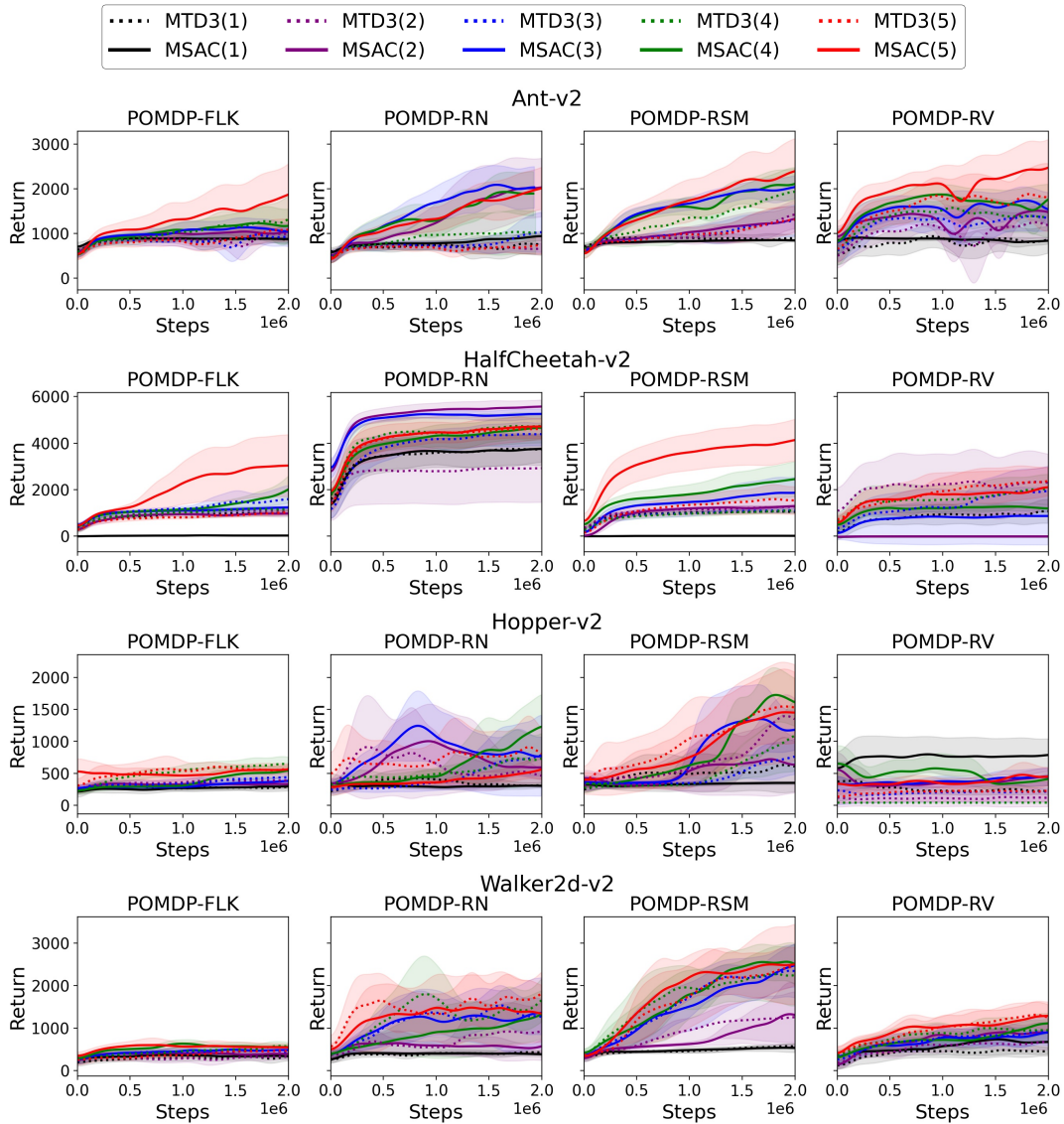


Fig. 2: Effect of Multi-step Size on The Performance of MTD3 and MSAC, where the average learning curves correspond to MTD3(n) and MSAC(n) with different multi-step sizes n and the shaded area shows half of standard deviation of the average accumulated return over 3 random seeds.

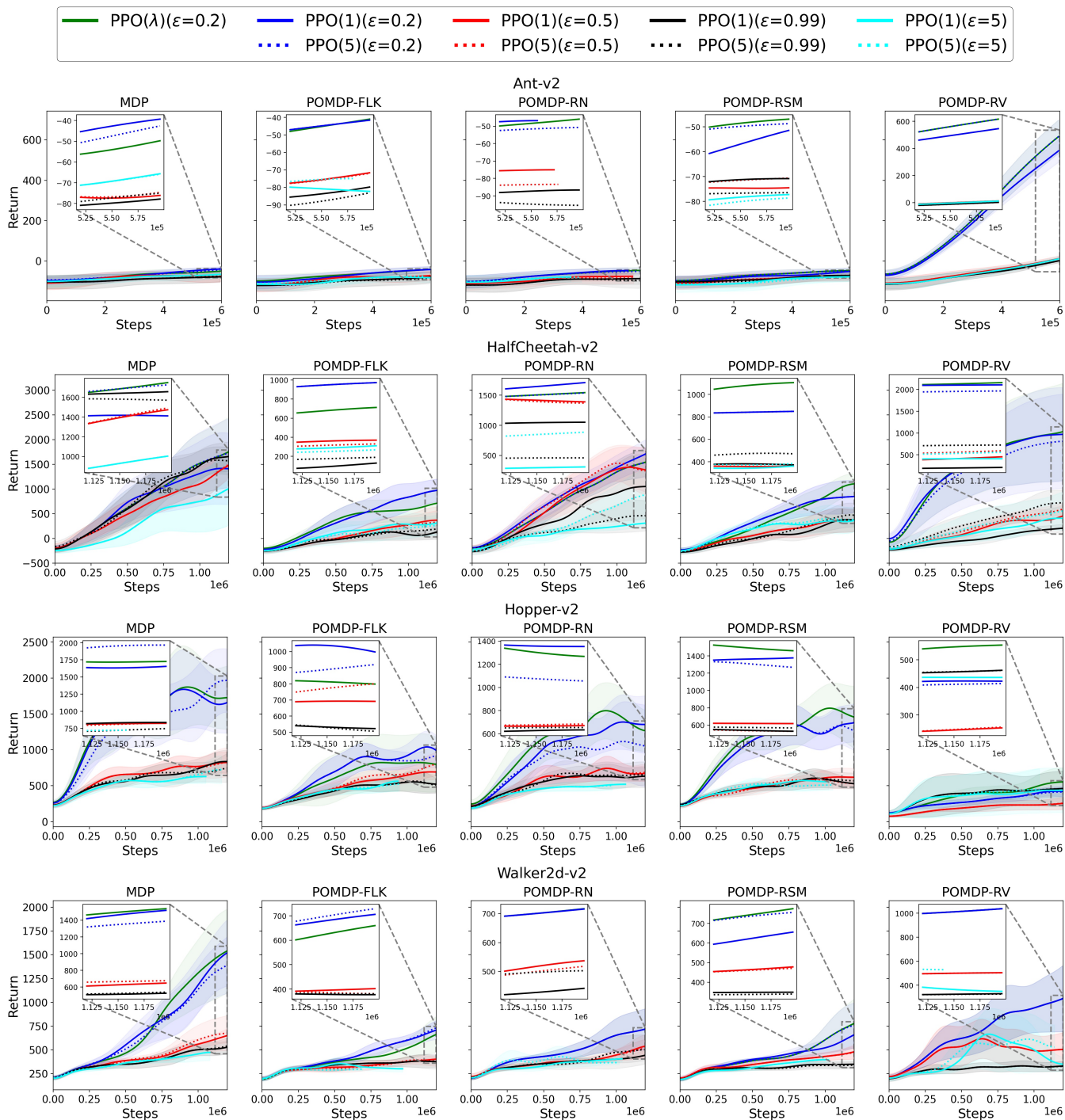


Fig. 3: Effect of Multi-step Size on The Performance of PPO, where the average learning curves correspond to PPO(λ) with λ -return and PPO(n) with simple n -step bootstrapping and the shaded area shows half of standard deviation of the average accumulated return over 3 random seeds. The ϵ indicates how far away the new policy is allowed to go from the current one.